The Journal of Chemical Physics

RESEARCH ARTICLE | APRIL 04 2023

DEHP$^-$ extractant binding to trivalent lanthanide Er^{3+}: Fast binding accompanied by concerted angular motions of hydration water

Zhu Liang ; Trung Vo ; Karl J. Schweighofer ; Ilan Benjamin ; Mark L. Schlossman

J. Chem. Phys. 158, 134715 (2023)
https://doi.org/10.1063/5.0138019

AIP Publishing

The Journal of Chemical Physics ARTICLE scitation.org/journal/jcp

$DEHP^-$ extractant binding to trivalent lanthanide Er^{3+}: Fast binding accompanied by concerted angular motions of hydration water

Cite as: J. Chem. Phys. 158, 134715 (2023); doi: 10.1063/5.0138019
Submitted: 7 December 2022 • Accepted: 13 March 2023 •
Published Online: 4 April 2023

Zhu Liang,[1,a] Trung Vo,[1] Karl J. Schweighofer,[2] Ilan Benjamin,[2,b] and Mark L. Schlossman[1,b]

AFFILIATIONS

[1] Department of Physics, University of Illinois at Chicago, 845 W. Taylor St., Chicago, Illinois 60607, USA
[2] Department of Chemistry and Biochemistry, University of California at Santa Cruz, Santa Cruz, California 95064, USA

[a] **Current address:** Center for Functional Nanomaterials, Brookhaven National Laboratory, Upton, NY 11973, USA.
[b] **Authors to whom correspondence should be addressed:** ilan@ucsc.edu and schloss@uic.edu

ABSTRACT

Solvent extraction of trivalent rare earth metal ions by organophosphorus extractants proceeds via binding of phosphoric acid headgroups to the metal ion. Water molecules in the tightly bound first hydration shell of the metal ions must be displaced by oxygen atoms from phosphoric acid headgroups. Here, we use classical molecular dynamics simulations to explore the event in which a fully hydrated Er^{3+} binds to its first phosphoric acid headgroup. Approach of the headgroup into the region between the first and second hydration shells leads to a fast ejection of a water molecule that is accompanied by reordering of the hydration water molecules, including discretization of their angular positions and collective rotation about the metal ion. The water molecule ejected from the first shell is located diametrically opposite from the binding oxygen. Headgroup binding places a headgroup oxygen closer to Er^{3+} than its first hydration shell and creates a loosely bound water that subsequently exchanges between the first shell and its environment. This second exchange of water also occurs at discrete angular positions. This geometrical aspect of binding may be of relevance to understanding the binding and transport of ion–extractant complexes that are expected to occur at the organic–aqueous liquid–liquid interface used in solvent extraction processes.

I. INTRODUCTION

Numerous chemical and biomolecular binding processes that take place in aqueous solutions involve the replacement of water molecules in a hydration layer by the binding moiety. In the case of relatively weakly bound hydration water, the more strongly interacting binding moiety can easily exchange with a hydration water molecule. Strongly bound hydration layers, such as those of multivalent ions may be less malleable and provide a barrier to binding. We investigate the binding of an extractant molecule to a trivalent lanthanide, a process of relevance to the separation and purification of rare earth elements.[1] Although hydration water molecules are strongly bound to Er^{3+}, $\Delta G_{solv} = -3495$ kJ mol^{-1},[2] we find that the ease of circumferential rotation of water molecules about Er^{3+} allows for concerted motions that accompany a swift binding of extractant to ion.

Early molecular dynamics (MD) studies of the static structure and dynamics of the hydration layer of trivalent lanthanides, which included studies of the exchange of water molecules between the first and second hydration shells and bulk water, are closely related to this study. This pioneering work revealed that the first hydration shell of a light lanthanide, Nd^{3+}, contained nine water molecules arranged in a tricapped trigonal prism (TTP) geometry, whereas the first hydration shell of a heavy lanthanide, Yb^{3+}, contained eight water molecules in a square antiprism.[3] Water exchange events were recorded during which a water molecule from the first hydration shell moved to the second and a water molecule from the second hydration shell moved to the first. Broadly speaking, these events are categorized in terms of three mechanisms: (1) dissociative, in which a water molecule moves out of the first shell, then afterward a second water molecule moves in, (2) associative, in which a water molecule from the second shell moves into the first, then afterward a water molecule from the first shell moves to the second, or (3) an interchange process during which the two exchanges occur simultaneously. Dissociative events have an intermediate first hydration shell

with a decreased coordination number (CN), whereas associative events have an intermediate with increased CN. Variations of these simple categories have been observed. For example, water exchange events for $[Nd(H_2O)_9]^{3+}$ were assigned a dissociative activated interchange, I_d, mechanism, in which the intermediate state has decreased coordination, CN = 8, but also has a preferential arrangement of the exchanging water molecules of 180° in which they are located on opposite sides of the Nd^{3+} ion.[4] The lifetime of the intermediate CN = 8 square antiprism varied between 0 and 10 ps.

As reviewed by D'Angelo and Spezia, lighter trivalent lanthanides have nine water molecules in the first shell and the heaviest have 8, with some intermediate lanthanides having non-integer values that indicate a dynamic equilibrium between eightfold and ninefold structures.[5] This is believed to be driven largely by the ion size that contracts along the lanthanide series. Recent high-precision x-ray absorption spectroscopy (XAS) measurements, which resolved some erratic behavior in previously reported Ln-O distances, indicated that the crossover from 9 to 8 does not occur near the center of the lanthanide series, that is, at Sm, as often claimed, but occurs at heavier lanthanides.[6] These measurements indicated that the coordination number should be 8.9 ± 0.5 for the Er^{3+} studied here, though a recent XAS measurement yielded 7.9 ± 0.2,[7] and a similar value of eight water molecules was obtained from HEXS.[8] The XAS studies also revealed a preference for hydration water to form a trigonal tricapped prism structure for CN = 9 and a square antiprism structure for CN = 8 in the heavier lanthanides, though accompanying *ab initio* MD simulations point to dynamic coordination geometries.[7,9,10]

These studies of hydration shell structure and water exchange provide the basis to understand binding events in which hydrated trivalent lanthanides bind to other molecules, for example, for the purpose of separating or purifying them. Solvent extraction is a hydrometallurgical technique used for the separation and purification of rare earth elements.[11] Extractant molecules assist the transport of selected lanthanides from a multi-component aqueous mixture into an organic solvent. Early studies of the solvent extraction of lanthanide elements, which make up most of the rare earth elements, demonstrated the utility of organophosphoric acid extractants, such as bis(2-ethylhexyl) phosphoric acid (HDEHP) dissolved in organic solvents.[12] When the organic phase is placed in contact with an immiscible aqueous phase of lanthanides, HDEHP complexes with lanthanide ions and extracts them into the bulk organic phase.[13] In addition to its organic solubility, HDEHP is partially soluble in water and interactions of lanthanide ions with HDEHP in an aqueous phase have been studied recently.[14–16] It has been suggested that interactions of HDEHP with lanthanide ions at both the aqueous–organic interface and the aqueous phase can be relevant for solvent extraction.[16]

Solvent extraction of lanthanides (Ln) by HDEHP is known to proceed through the following reaction:[17]

$$Ln^{3+}\,(a) + 3(HX)_2\,(o) \rightleftarrows Ln[(HX)_2]_3(o) + 3H^+\,(a), \quad (1)$$

where X refers to deprotonated HDEHP, that is, $DEHP^-$, HX refers to HDEHP, and (a) and (o) refer to the aqueous and organic phases, though as mentioned above HDEHP can also be found in the aqueous phase. Lanthanide ion binding to extractants involves the displacement of some or all hydration water molecules, which are not explicitly represented in Eq. (1). Mechanistic aspects on the molecular scale of assisted ion transport across the aqueous–organic liquid–liquid interface are mostly unknown, though recent simulations and experiments have started to explore multi-molecular interfacial processes that contribute to the transport.[18–21] Although it is likely that the binding of a hydrated lanthanide to extractant occurs primarily at the aqueous–organic interface, here we present a simplified model of the first step of that process by using classical MD simulations to investigate Er^{3+} binding to a single $DEHP^-$ in water. Subsequent publications will report simulations of this process at the liquid–liquid interface and this work will serve as a basis of comparison.

II. METHODS

Classical molecular dynamics (MD) simulations utilized Desmond software.[22] Our MD system contained 4071 water molecules, one erbium ion, Er^{3+}, one deprotonated HDEHP molecule ($DEHP^-$), and two Cl^- ions. Chloride ions did not participate in binding and were included for the electrical neutrality of the system. The simulation box was cubic, 50 Å in each direction. Periodic boundary conditions were applied in all directions.

Water molecules were described by the simple point charge (SPC) model.[23] The $DEHP^-$ molecule shown in Chart 1 was modeled using the OPLS-UA force field,[24] while the potentials for Er^{3+} were modeled using parameters that reproduce the ion-oxygen distance.[25] The Er–water interaction potential was optimized to a non-polarizable water model and reproduces quite well the structure of the hydration complex. This choice for the water and the water–Er interaction potentials is motivated by the requirement that these potentials reproduce the experimentally available Er–O distances measured in bulk water. They also reproduce, within the experimental statistical uncertainty, the Er coordination number in bulk water.

Non-bonded interactions were described with conventional 12-6 Lennard-Jones (L-J) and Coulombic pairwise interactions,

$$u_{ij}(r) = 4\varepsilon_{ij}\left[\left(\frac{\sigma_{ij}}{r}\right)^{12} - \left(\frac{\sigma_{ij}}{r}\right)^{6}\right] + \frac{q_i q_j}{4\pi r \varepsilon_0}, \quad (2)$$

where r is the distance between atom centers i and j. Standard Lorentz–Berthelot combining rules, $\sigma_{ij} = (\sigma_i + \sigma_j)/2$ and $\varepsilon_{ij} = (\varepsilon_i \varepsilon_j)^{1/2}$, were used to generate Lennard-Jones parameters for all mixed interactions. Electrostatics were calculated with the

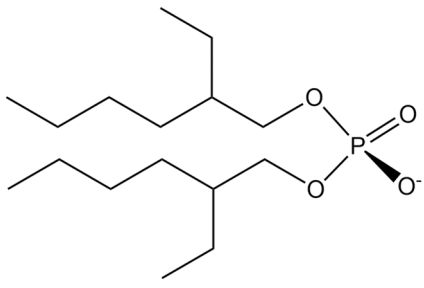

CHART 1. Molecular structure of $DEHP^-$.

u-series method.[26] Long-range Lennard-Jones and electrostatics interactions were cut off at 9 Å.

Radial distribution functions $g(r)$ at T = 300 K were calculated in the presence and absence of $DEHP^-$. Calculations in the absence of $DEHP^-$ included 4106 water molecules and an additional Cl^- ion for electrical neutrality and were run for 10 ns. When $DEHP^-$ was present, calculations were run for 10 ns after $DEHP^-$ and Er ion were bound at a metal–phosphorus distance of roughly 3.6 Å. Coordination numbers CN were calculated using

$$\langle n(r)\rangle = \int_0^r 4\pi\rho_W g(r) r^2 dr, \tag{3}$$

where ρ_W is the bulk water density (0.033 $Å^{-3}$). The value of the integral near the minima of $g(r)$ determined the ion's coordination number CN. For example, its value at r = 3.5 Å, close to the minimum between the first and second hydration shells, was used to determine CN of the first hydration shell.

The potential of mean force was calculated as a function of distance r_{Er-P} from the P atom of $DEHP^-$ to the Er^{3+} ion by utilizing the WHAM method.[27–29] We restrained the distance r_{Er-P} in a harmonic potential with a force constant of 50 kcal mol^{-1} $Å^{-2}$. A step size of 0.1 Å was used when changing r_{Er-P} from 8 to 3 Å. Each step was run for 2 ns at a constant temperature of 300 K. The free energy was calculated from

$$A(r_{Er-P}) = -k_B T \ln P_{ub}(r_{Er-P}), \tag{4}$$

where k_B is the Boltzmann constant, T is the temperature of the simulation, and $P_{ub}(r_{Er-P})$ is the unbiased distribution of Er–phosphorus distances.

Simulations of the binding dynamics with $DEHP^-$ consisted of a two-step process. First, a longer simulation was run to create a set of seed configurations from which a series of shorter simulations were run to observe the binding process. The longer simulation was run for 10 ns with the distance between Er^{3+} and the deprotonated oxygen of $DEHP^-$ constrained in a harmonic potential centered at 4 Å with a force constant of 10 kcal mol^{-1} $Å^{-2}$. A snapshot of the system trajectory was saved every 100 ps, yielding 100 snapshots in total as the initial seeds for the simulations that followed. These snapshots provided a range of initial distances r_{Er-P} shown in Fig. 1. Starting from each of the 100 seeds, a 240 ps simulation was run 100 times with an initially random seed velocity. No constraints were used in these short simulations to ensure that the $DEHP^-$ head group moved freely. This resulted in 10 000 simulations that formed the dataset for the analysis of binding dynamics. The extractant $DEHP^-$ bound to Er^{3+} in 1506 of the 10 000 simulations (Fig. 1).

III. RESULTS AND DISCUSSION

Binding of the deprotonated bis(2-ethylhexyl) phosphoric acid ($DEHP^-$) extractant to trivalent Er^{3+} in bulk water was calculated by classical MD simulations as described in Sec. II. Figure 2 (Multimedia view) illustrates three snapshots from a typical binding event. Figure 2(a) occurs −3.06 ps before the binding illustrated in Figs. 2(b) and 2(c) occurs 2.64 ps afterward. The progress of the binding event is measured by the reaction coordinate ξ, where $\xi = r_{O(H_2O^{ej})-Er} - r_{P-Er}$. Here, $r_{O(H_2O^{ej})-Er}$ is the distance from the center of the Er ion to the center of the oxygen atom of the water molecule that is ejected during the binding process and r_{P-Er} is the distance from the center of Er to the center of the phosphorus in the $DEHP^-$ headgroup. The reaction coordinate ξ is negative prior to the binding event and positive afterward. The time t = 0 of the binding event is defined as the MD frame immediately prior to the frame in which r_{P-Er} becomes smaller than 4.3 Å for reasons that will be described later. The MD frame duration is 60 fs. Figure 2 (Multimedia view) shows a typical binding event when the Er ion has nine water molecules in its first hydration shell. The ejected water molecule is located nearly diametrically opposite to the binding $DEHP^-$ oxygen atom.

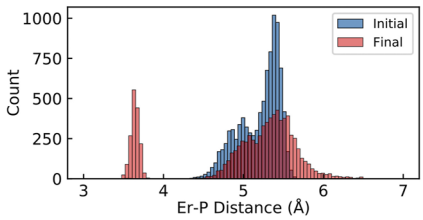

FIG. 1. Initial and final distributions of the distance r_{Er-P} for the 10 000 simulations that formed the dataset for the analysis of binding dynamics. The final distribution in red shows bound configurations for r_{Er-P} near 3.6 Å and unbound configurations further away.

A. Static structure near the Er ion

Figure 3 shows the radial distribution function $g(r)$ for oxygen atoms near Er^{3+} in the absence and presence of $DEHP^-$. In the absence of $DEHP^-$, the centers of the peaks of the two hydration shells are located at r = 2.355 Å and r = 4.53 Å. These are consistent with measured values of 2.354 ± 0.004 and 4.55 ± 0.04 Å.[7] The coordination number of water molecules in the first hydration shell, CN = 9.0, is larger than a recent XAS measurement of 7.9 ± 0.2,[7] and a similar value of eight water molecules obtained from HEXS,[8] but consistent with another recent XAS measurement of 8.9 ± 0.5.[6]

The blue line in Fig. 3 shows the Er–O $g(r)$ after $DEHP^-$ is bound to Er. A small peak at 2.17 Å represents one oxygen from $DEHP^-$ that is bound to Er. This oxygen binds closer to Er than water molecule oxygen atoms because the partial charge of −0.97 e on the bound $DEHP^-$ oxygen is more negative than the partial charge of −0.82 e on the water oxygen. A larger peak at 2.34 Å represents 7.7 O atoms from water molecules that remain in the first hydration shell. These numbers are consistent with the green line in Fig. 3, which shows the Er–O $g(r)$ for only water molecules after $DEHP^-$ binds to Er. The position of the second hydration shell of water is 4.51 Å, which also includes the location of the three remaining oxygen atoms from $DEHP^-$. The radii of the water hydration shells are essentially the same with and without $DEHP^-$.

The coordination numbers in Fig. 3 indicate that prior to binding $DEHP^-$ approaches an Er ion with nine water molecules in its first hydration shell. As discussed later, analysis of the bound complex within a few simulation frames of binding (each frame is 60 fs) reveals eight water molecules in the first hydration shell, consistent with the ejection of one water molecule as shown in Fig. 2 (Multimedia view). However, analysis at later times reveals that one

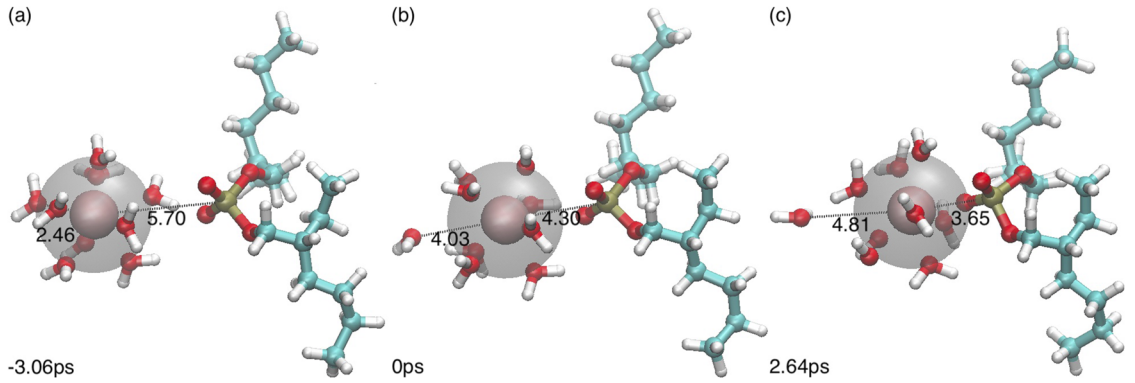

FIG. 2. Illustration of the binding of $DEHP^-$ and ejection of a hydration shell water molecule from Er^{3+} in bulk water. The gray sphere is used to illustrate the radial position of the hydration shell. It is centered on Er^{3+} with a radius of 2.35 Å. (a) $t = -3.06$ ps, $\xi = -3.24$ Å, (b) $t = 0$ ps, $\xi = -0.27$ Å, and (c) $t = 2.64$ ps, $\xi = 1.16$ Å, where the reaction coordinate $\xi = r_{O(H_2O^{ej})-Er} - r_{P-Er}$. The ejection angle in (c) between the vectors Er–P and $O(H_2O^{ej})$–Er is 160°. A movie of this event is available in the SM. Multimedia view: https://doi.org/10.1063/5.0138019.1.

water molecule is loosely bound, which produces either seven or eight water molecules in the first shell. Any one of the eight water molecules appears equally likely to be loosely bound. These observations are consistent with the coordination number of 7.7 water molecules in the first shell shown in Fig. 3.

The Er–P $g(r)$ shown in Fig. 3 illustrates a position of 3.63 Å for the P of the bound $DEHP^-$ with a coordination number of 1. Figure 4 illustrates the potential of mean force (PMF) for a range of Er–P distances. The minimum is at 3.66 Å, consistent with the $g(r)$ simulation. The energy barrier to binding is 1.81 kcal/mol, which is calculated from the minimum at 5.38 Å and the maximum at 4.40 Å.

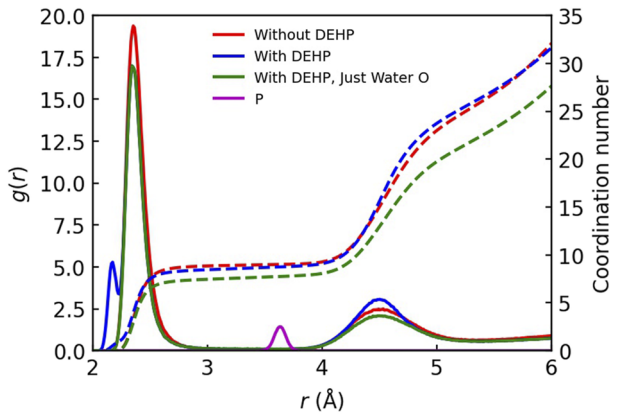

FIG. 3. Radial distribution function $g(r)$ of Er–O and Er–P distances. Solid lines show the $g(r)$; dashed lines show the coordination number for the $g(r)$ of Er–O. The red line ("without DEHP") shows the result of calculations with only Er^{3+}, Cl^-, and water. The blue and green lines often overlap and show results for Er^{3+} bound to $DEHP^-$, but the green line shows the result for oxygen atoms only from water molecules whereas the blue line also includes oxygen atoms from the $DEHP^-$ that binds to Er(III). The purple line shows the Er–P $g(r)$. The coordination number for P is 1 (not shown).

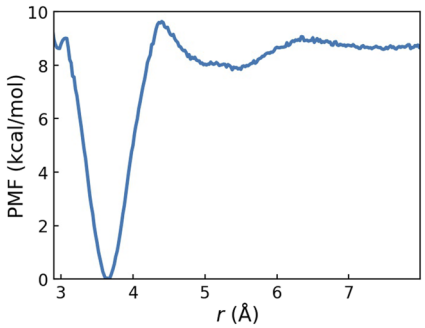

FIG. 4. Potential of mean force calculated as a function of the Er–P distance. The minimum at 3.66 Å was adjusted to 0 kcal/mol. Other relevant values include 9.64 kcal/mol at the barrier top near 4.40 Å, 7.83 kcal/mol at the minimum at 5.38 Å, and 9.07 kcal/mol at the secondary maximum at 6.34 Å, and 8.61 kcal/mol at 7.5 Å.

The binding energy calculated from the values at 7.5 and 3.66 Å is 8.61 kcal/mol.

B. Water dynamics during $DEHP^-$ binding to Er^{3+}

Figure 5 illustrates the dynamics of simulation trajectories that produce a bound $DEHP^-$–Er^{3+} complex in a bulk water environment. The dashed line in Fig. 5 shows the coordination number CN of water molecules in the first hydration shell of Er^{3+} as the binding reaction proceeds. At time $t = 0$ in the trajectory, a water molecule has been ejected: the CN has dropped to a value of 8, which is a reduction of one water molecule from the CN of 9.0 of an isolated Er^{3+} ion in bulk water (shown in Fig. 3). Over a span of roughly ±600 fs before and after the threshold, for a total of 1.2 ps, the CN drops rapidly from 8.7 to 7.9. The shoulder in the plot at frame 0 reveals a short-term stability of the $DEHP^-$–Er^{3+} complex with eight water molecules, which lasts roughly 0.3 ps. At later times, the CN of

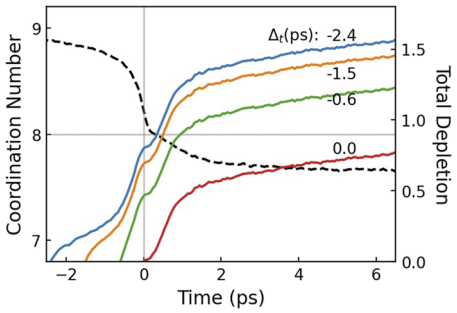

FIG. 5. First hydration shell water dynamics during the binding of $DEHP^-$ to Er^{3+}. Each curve represents an average over the 1506 trajectories that exhibited binding. The black dashed line is the coordination number CN of water molecules in the first hydration shell defined for water molecules whose Er–O distance is less than 3.5 Å. The time $t = 0$ is defined as the MD frame immediately prior to the frame at which r_{P-Er} becomes less than 4.3 Å. The solid-colored lines represent the total depletion h_{tot} for different values of Δ_t.

7.7 indicates that roughly 30% of the $DEHP^-$–Er^{3+} complexes contain seven water molecules and the other 70% contain 8 in the first hydration shell.

The solid lines in Fig. 5 present the average of h_{tot} over all the trajectories that ended with binding of $DEHP^-$ to Er^{+3}. The total depletion h_{tot} is calculated as follows: (i) at time $t = -\Delta_t$, (relative to $t = 0$) every water molecule i inside the Er^{+3} first hydration shell is assigned the value $h_i = 0$; (ii) h_i is switched to 1 when the water molecule i leaves the Er^{+3} hydration shell; and (iii) $h_{tot}(t) = \Sigma\, h_i(t)$. The figure shows a monotonically rising value of h_{tot}, indicating that the original set of water molecules in the first shell is progressively depleted. Independent of the choice of Δ_t, the most rapid rate of depletion occurs within a span of ±600 fs on either side of $t = 0$, which corresponds to the behavior observed for the coordination number. The small plateau in the plot near $t = 0$ is consistent with the short-term stability of a $DEHP^-$–Er^{3+} complex with eight water molecules, as also observed for the coordination number. Finally, the comparison of the rise in h_{tot} after roughly $t = 1.5$ ps and the nearly stable value of CN = 7.7 suggests that water molecules moving in from outside the first shell compensate for the loss of water molecules originally in the first shell.

C. Phosphorus dynamics during $DEHP^-$ binding to Er^{3+}

The potential of mean force in Fig. 4 exhibits a barrier peak at $r_{P-Er} = 4.4$ Å. As demonstrated above, roughly one water molecule has been ejected from the first hydration shell of Er^{3+} by $t = 0$, that is, the simulation frame just before the distance r_{P-Er} drops below 4.3 Å. Note that this $t = 0$ frame consists of distances r_{P-Er} very close to the peak in the potential of mean force. Given our somewhat coarse time resolution of 60 fs, an estimate of the transmission coefficient k of the binding process is calculated as follows: (i) set $k = 1$ when r_{P-Er} first crosses below a threshold value (e.g., 4.3 Å), and (ii) let $k = 1$ if r_{P-Er} is below the threshold, but set k to 0 if r_{P-Er} exceeds the threshold. The threshold is selected near the top of the barrier height shown in Fig. 4 as is customary in chemical reaction barrier crossing dynamics. However, given the uncertainty in the exact location of the barrier, we examined the sensitivity of the transmission coefficient to this choice.

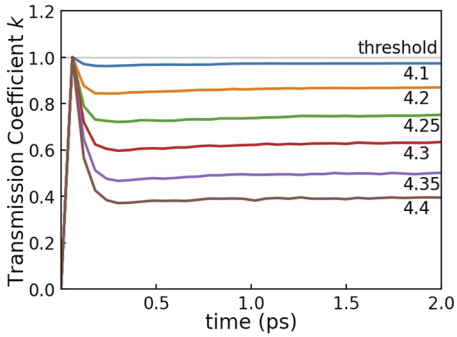

FIG. 6. Average value of the time-dependent transmission coefficient k for different values of the threshold distance r_{P-Er} in angstroms. The curves represent an average over all trajectories that reach the threshold value.

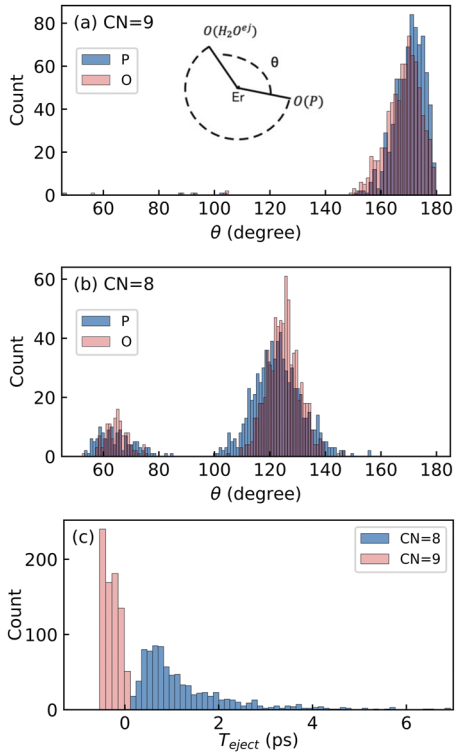

FIG. 7. Angular distribution of ejected water molecules measured with respect to either the oxygen (bound to Er) or the phosphorus atom of $DEHP^-$ molecules that bind to Er^{3+}. (a) Water molecules ejected from a first hydration shell containing nine water molecules. The inset defines the angle θ between the oxygen atom of the water molecule that will be ejected and the bound oxygen or phosphorus atom of $DEHP^-$. (b) Water molecules ejected from a first hydration shell containing eight water molecules. (c) Frames when CN = 8 and CN = 9 water ejection events occur.

The time dependence of k reflects the possibility that the trajectory (even once reaching the transition state) does not always

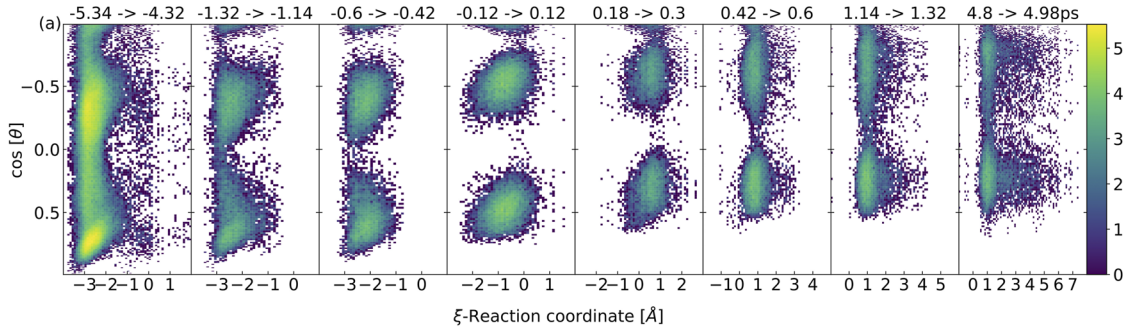

FIG. 8. Reaction coordinate ξ-angle heat map for successive intervals of time t in ps identified above each panel. Recall that $\xi = d_{O(H_2O^{ej})-Er} - d_{P(DEHP)-Er}$. The angle θ is measured between the Er–O(water) vector and the Er–P(DEHP) vector, where P(DEHP) is the phosphorus atom from $DEHP^-$. The heat map includes all water molecules that are in the first hydration shell at $t = -0.6$ ps. Color scale is ln(counts).

continue straight to binding and may experience reversal and recrossings. The time-dependent transmission coefficient is shown in Fig. 6, which demonstrates that more than roughly 35% of binding reactions are reversed at a threshold of $r_{P-Er} = 4.3$ Å, though very little reversal takes place at a smaller threshold of $r_{P-Er} = 4.1$ Å. The reversal takes place within 60 to 120 fs, indicating that the barrier height is similar to those typically found in chemical reactions in solution that involved chemical bond breaking with short relaxation times (<100 fs).[30] Since the barrier top is at 4.3 to 4.4 Å, k is underestimated when the threshold is placed at smaller distances since trajectories that reach this distance are already on their way to bind.

Figure 2 (Multimedia view) illustrated a binding event for which the ejected water molecule was nearly diametrically opposite to the binding O(P) atom. Figure 7 illustrates that this is the predominant geometry of water ejection that occurs just prior to $t = 0$ when the P atom approaches within $r_{P-Er} = 4.3$ Å. Figure 7(a) shows the distribution of water ejection angles calculated by starting at $t = -0.6$ ps, then identifying the first water molecule whose distance $r_{O(water)-Er}$ exceeds 3.5 Å for at least two frames. Note that changing the criterion to ten frames does not alter the angular distribution greatly. Figure 7(a) counts only those water molecules ejected from a first hydration shell containing nine water molecules in the simulation frame prior to ejection. Angles and coordination numbers are recorded from the simulation frame that precedes the ejection of a water molecule in the first hydration shell. It is observed that the ejection angle is highly anisotropic with a peak in the angular distribution close to 170°.

Figure 7(b) illustrates a very different angular distribution when water molecules are ejected from a first hydration shell containing eight water molecules. Figure 7(c) shows that these ejection events arise exclusively at later frames than those observed in Fig. 7(a); specifically, CN = 8 ejection events occur for positive frames, whereas CN = 9 ejection events occur for negative frames. Recalling that on average one water molecule has already been ejected at frame 0 from a first hydration shell with 9.0 water molecules, most of the CN = 8 water ejections shown in Fig. 7 consist of a second water molecule ejected from the hydration shell. This is consistent with the average drop in water coordination below CN = 8 observed in Fig. 5 for positive frames.

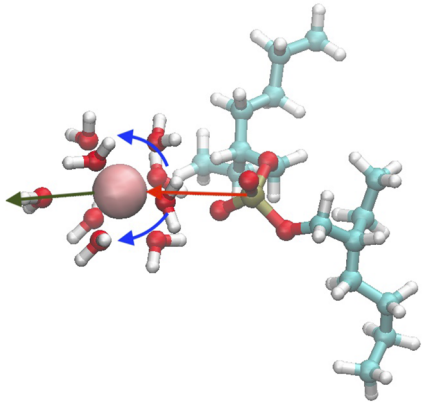

FIG. 9. Schematic representation of atomic motions during $DEHP^-$ binding to Er^{3+}. The red arrow illustrates the incoming P, the green arrow illustrates the outgoing water molecule, and the blue arrows show the direction of rotation of water molecules that remain in the first hydration shell.

A collective rearrangement of water molecules in the first hydration shell occurs as the binding takes place. Figure 8 illustrates the angle of every water molecule in the hydration shell as a function of the reaction coordinate $\xi = r_{O(H_2O^{ej})-Er} - r_{P-Er}$ for approach of $DEHP^-$ to Er with CN = 9 where the coordination number is determined at $t = -0.6$ ps. The colors represent the number of water molecules at a particular reaction coordinate and angle. The panels represent all the water molecules in the first hydration shell, where each panel illustrates a successive interval of time.

Figure 8 shows that the angular distribution becomes more discrete as the binding event time varies from −5 to 0 ps. In addition, the polar angle θ of the water molecules in the hydration shell increases as the binding reaction proceeds. For example, between −5.34 and −4.32 ps, there are three highly occupied clusters of angular positions, at $\xi = -3.0$ and 40° ($\cos\theta = 0.77$), 109° ($\cos\theta = -0.33$), and at $\xi = -2.7$ and 165° ($\cos\theta = -0.97$), but water molecules are located at nearly all angular positions to some extent. Close to 0 ps and $\xi = -1$, the angular positions of the

water molecules have increased to roughly 60° ($\cos\theta$ = 0.50) and 120° ($\cos\theta$ = −0.5), with some water molecules remaining near 180°. The collective angular changes (illustrated schematically in Fig. 9) continue as the binding proceeds until about 0.5 ps when the angular distribution stabilizes with only two clusters of angular positions centered at 71° ($\cos\theta$ = 0.33) and 125° ($\cos\theta$ = −0.57). At that time, the oxygen of the $DEHP^-$ has fully replaced the ejected water molecule within the hydration shell. At subsequent times, a tail develops, which extends from these peaks to larger values of ξ. The tails represent water molecules in the first hydration shell at a time when the ejected water molecule, whose position appears in the reaction coordinate, has moved much further away from Er.

IV. CONCLUSION

The extractant HDEHP is commonly used in rare earth processes to extract lanthanides like Er.[31] This extraction is expected to involve a series of binding events in which $DEHP^-$ extractants replace water molecules in the first hydration shell of Er^{3+}. As the first stage of a project to understand the mechanism of the binding and transport of Er^{3+} from an aqueous to an organic phase, we have used MD simulations to study a single binding event of $DEHP^-$ to fully hydrated Er^{3+} in bulk water.

The binding proceeds quickly, despite the large hydration-free energy of Er^{3+}. Like the concerted electronic motions that occur in chemical reactions, the fast binding is accompanied by concerted motions of water molecules throughout the first hydration shell. Upon approach of $DEHP^-$ to Er^{3+}, water molecules in the first hydration shell undergo a collective rotation about Er^{3+} that is directed away from the entering oxygen of the $DEHP^-$. Tightly bound hydration water molecules reside within a roughly spherical but deep potential well about the ion, which allows for a facile rearrangement of their angular positions but constrains radial motions. Accompanying this collective rotation is the ejection of a water molecule that occurs while the $DEHP^-$ headgroup is still in the region between the first and second hydration shells. The remaining water molecules in the first hydration shell distribute themselves at discrete polar angles with respect to the incoming P or O of the $DEHP^-$.

Figure 7 showed that the first water molecule ejected is roughly 170° away from the incoming P or O of the $DEHP^-$. Presumably, the angular motion of water molecules directed away from the position of the entering O(P) creates stress on the water molecule diametrically opposite to the entering O(P), which is the water molecule ejected during most of the binding events when nine water molecules are in the first hydration shell. Binding of $DEHP^-$ places one of its oxygen atoms closer to Er^{3+} than the first hydration shell. Shortly after binding, the average CN of water molecules in the first hydration shell is CN = 7.7. This shows a loose association of one of the water molecules in the hydration shell and Fig. 7 showed that a second water molecule can be ejected, primarily at an angle of roughly 120°. Far fewer water molecules are ejected at 60°, which may indicate that the bulky $DEHP^-$ influences the ejection of water molecules closest to it.

The binding event is dissociative because a water molecule is ejected before $DEHP^-$ fully binds to the Er^{3+}. Evidence for this is provided in Fig. 5 where the average CN has dropped to 8, yet the P is still 4.3 Å from Er. Once fully bound, P will be at 3.63 Å as shown in Fig. 3. However, it may be preferable to consider the event as a dissociative activated substitution, I_d, because of the preferential ejection angle of the ninth water molecule, as well as the angular discretization of water molecules in the first hydration shell with respect to the incoming O (or P) of the $DEHP^-$. This nomenclature is consistent with that previously assigned to water exchange events for $[Nd(H_2O)_9]^{3+}$ for similar reasons as mentioned in Sec. I.[4]

The specific geometrical and collective nature of this binding event may be indicative of related aspects of binding additional $DEHP^-$ that are required to extract lanthanides in a solvent extraction process. This geometrical aspect of binding may also be of relevance to understanding the binding and transport of ion–extractant complexes that are expected to occur at the asymmetric organic–aqueous liquid–liquid interface utilized in solvent extraction processes.

ACKNOWLEDGMENTS

This research was performed using funding received from the U.S. Department of Energy, Office of Science, Office of Basic Energy Sciences Separations Program (Award No. DE-SC0018200) to M.L.S. and I.B..

AUTHOR DECLARATIONS

Conflict of Interest

The authors have no conflicts to disclose.

Author Contributions

Zhu Liang: Data curation (lead); Formal analysis (lead); Investigation (equal); Methodology (equal); Software (lead); Writing – original draft (supporting); Writing – review & editing (supporting). **Trung Vo**: Data curation (supporting); Formal analysis (supporting); Software (supporting); Writing – original draft (supporting); Writing – review & editing (supporting). **Karl J. Schweighofer**: Methodology (supporting); Software (supporting). **Ilan Benjamin**: Conceptualization (lead); Formal analysis (equal); Investigation (equal); Methodology (lead); Resources (equal); Supervision (equal); Writing – original draft (supporting); Writing – review & editing (supporting). **Mark L. Schlossman**: Conceptualization (lead); Formal analysis (supporting); Funding acquisition (lead); Methodology (equal); Project administration (equal); Software (equal); Writing – original draft (lead); Writing – review & editing (lead).

DATA AVAILABILITY

The computational data that support the findings of this study are available from the corresponding authors upon reasonable request.

REFERENCES

[1] P. A. Tasker, P. G. Plieger, and L. C. West, "Metal complexes for hydrometallurgy and extraction," in *Comprehensive Coordination Chemistry II: From Biology*

to Nanotechnology, edited by J. A. McCleverty and T. J. Meyer (Elsevier, Oxford, 2004), Vol. 9, p. 759.
[2]Y. Marcus, "A simple empirical model describing the thermodynamics of hydration of ions of widely varying charges, sizes, and shapes," Biophys. Chem. **51**, 111 (1994).
[3]T. Kowall, F. Foglia, L. Helm, and A. E. Merbach, "Molecular dynamics simulation study of lanthanide ions Ln^{3+} in aqueous solution. Analysis of the structure of the first hydration shell and of the origin of symmetry fluctuations," J. Phys. Chem. **99**, 13078 (1995).
[4]T. Kowall, F. Foglia, L. Helm, and A. E. Merbach, "Mechanisms of water exchange between lanthanide(III) aqua ions $[Ln(H_2O)_n]^{3+}$ and bulk water: A molecular dynamics simulation approach including high-pressure effects," Chem. -Eur. J. **2**, 285 (1996).
[5]P. D'Angelo and R. Spezia, "Hydration of lanthanoids(III) and actinoids(III): An experimental/theoretical saga," Chem. -Eur. J. **18**, 11162 (2012).
[6]P. D'Angelo, A. Zitolo, V. Migliorati, G. Chillemi, M. Duvail, P. Vitorge, S. Abadie, and R. Spezia, "Revised ionic radii of lanthanoid(III) ions in aqueous solution," Inorg. Chem. **50**, 4572 (2011).
[7]R. C. Shiery, J. L. Fulton, M. Balasubramanian, M.-T. Nguyen, J.-B. Lu, J. Li, R. Rousseau, V.-A. Glezakou, and D. C. Cantu, "Coordination sphere of lanthanide aqua ions resolved with ab initio molecular dynamics and x-ray absorption spectroscopy," Inorg. Chem. **60**, 3117 (2021).
[8]L. Soderholm, S. Skanthakumar, and R. E. Wilson, "Structures and energetics of erbium chloride complexes in aqueous solution," J. Phys. Chem. A **113**, 6391 (2009).
[9]I. Persson, P. D'Angelo, S. De Panfilis, M. Sandström, and L. Eriksson, "Hydration of lanthanoid(III) ions in aqueous solution and crystalline hydrates studied by EXAFS spectroscopy and crystallography: The myth of the 'gadolinium break,'" Chem. -Eur. J. **14**, 3056 (2008).
[10]P. D'Angelo, A. Zitolo, V. Migliorati, and I. Persson, "Analysis of the detailed configuration of hydrated lanthanoid(III) ions in aqueous solution and crystalline salts by using K- and L_3-edge XANES spectroscopy," Chem. -Eur. J. **16**, 684 (2010).
[11]J. Rydberg, M. C. Choppin, and G. R. Choppin, *Principles and Practices of Solvent Extraction* (Marcel Dekker, New York, 1992).
[12]D. F. Peppard, G. W. Mason, J. L. Maier, and W. J. Driscoll, "Fractional extraction of the lanthanides as their di-alkyl orthophosphates," J. Inorg. Nucl. Chem. **4**, 334 (1957).
[13]M. Nilsson and K. L. Nash, "A review of the development and operational characteristics of the TALSPEAK process," Solvent Extr. Ion Exch. **25**, 665 (2007).
[14]R. Kusaka and M. Watanabe, "The structure of a lanthanide complex at an extractant/water interface studied using heterodyne-detected vibrational sum frequency generation," Phys. Chem. Chem. Phys. **20**, 2809 (2018).
[15]R. Kusaka and M. Watanabe, "Stoichiometry of lanthanide–phosphate complexes at the water surface studied using vibrational sum frequency generation spectroscopy and DFT calculations," J. Phys. Chem. B **125**, 6727 (2021).
[16]P. Sun, E. A. Binter, Z. Liang, M. A. Brown, A. V. Gelis, I. Benjamin, M. K. Bera, B. Lin, W. Bu, and M. L. Schlossman, "Antagonistic role of aqueous complexation in the solvent extraction and separation of rare earth ions," ACS Cent. Sci. **7**, 1908 (2021).
[17]T. B. Pierce and P. F. Peck, "The extraction of the lanthanide elements from perchloric acid by di-(2-ethylhexyl) hydrogen phosphate," Analyst **88**, 217 (1963).
[18]B. Qiao, J. V. Muntean, M. Olvera de la Cruz, and R. J. Ellis, "Ion transport mechanisms in liquid–liquid interface," Langmuir **33**, 6135 (2017).
[19]Z. Liang, W. Bu, K. J. Schweighofer, D. J. Walwark, Jr., J. S. Harvey, G. R. Hanlon, D. Amoanu, C. Erol, I. Benjamin, and M. L. Schlossman, "A nanoscale view of assisted ion transport across the liquid–liquid interface," Proc. Natl. Acad. Sci. U.S.A. **116**, 18227 (2019).
[20]M. J. Servis and A. E. Clark, "Surfactant-enhanced heterogeneity of the aqueous interface drives water extraction into organic solvents," Phys. Chem. Chem. Phys. **21**, 2866 (2019).
[21]N. Kumar and A. E. Clark, "Unexpected inverse correlations and cooperativity in ion-pair phase transfer," Chem. Sci. **12**, 13930 (2021).
[22]K. J. Bowers, E. Chow, H. Xu, R. O. Dror, M. P. Eastwood, B. A. Gregersen, J. L. Klepeis, I. Kolossváry, M. A. Moraes, F. D. Sacerdoti, J. K. Salmon, Y. Shan, and D. E. Shaw, in presented at the Proceedings of the ACM/IEEE Conference on Supercomputing (SC06), Tampa, FL, 2006.
[23]H. J. C. Berendsen, J. P. M. Postma, W. F. Van Gunsteren, and J. Hermans, "Interaction models for water in relation to protein hydration," in*Intermolecular Forces*, edited by B. Pullman (D. Reidel Publishing Company, Dordrecht, 1981), p. 331.
[24]W. L. Jorgensen, J. D. Madura, and C. J. Swenson, "Optimized intermolecular potential functions for liquid hydrocarbons," J. Am. Chem. Soc. **106**, 6638 (1984).
[25]P. Li, L. F. Song, and K. M. Merz, "Parameterization of highly charged metal ions using the 12-6-4 LJ-type nonbonded model in explicit water," J. Phys. Chem. B **119**, 883 (2015).
[26]C. Predescu, A. K. Lerer, R. A. Lippert, B. Towles, J. P. Grossman, R. M. Dirks, and D. E. Shaw, "The *u*-series: A separable decomposition for electrostatics computation with improved accuracy," J. Chem. Phys. **152**, 084113 (2020).
[27]M. A. Hughes and V. Rod, "A general model to account for the liquid/liquid kinetics of extraction of metals by organic acids," Faraday Discus. Chem. Soc. **77**, 75 (1984).
[28]B. Roux, "The calculation of the potential of mean force using computer simulations," Comput. Phys. Commun. **91**, 275 (1995).
[29]P. Li, B. P. Roberts, D. K. Chakravorty, and K. M. Merz, Jr., "Rational design of particle mesh Ewald compatible Lennard-Jones parameters for +2 metal cations in explicit solvent," J. Chem. Theory Comput. **9**, 2733 (2013).
[30]J. T. Hynes, "The theory of reactions in solution," in *The Theory of Chemical Reaction Dynamics*, edited by M. Baer (Chemical Rubber, Boca Raton, FL, 1985), p. 171.
[31]F. Xie, T. A. Zhang, D. Dreisinger, and F. Doyle, "A critical review on solvent extraction of rare earths from aqueous solutions," Miner. Eng. **56**, 10 (2014).